JOIV : Int. J. Inform. Visualization, 7(3) - September 2023 839-846

INTERNATIONAL JOURNAL ON INFORMATICS VISUALIZATION

journal homepage : www.joiv.org/index.php/joiv

Analyzing Coverage Probability of Reconfigurable Intelligence Surface-aided NOMA

Agung Mulyo Widodo [a,b,*], Heri Wijayanto [c], I Gede Pasek Suta Wijaya [c], Andika Wisnujati [b,d], Ahmad Musnansyah [e]

[a] *Computer Science Faculty, Universitas Esa Unggul, West Jakarta, Indonesia*
[b] *Department of Computer Science, Asia University, Liufeng Road, Taichung City, Taiwan*
[c] *Informatics Study Program, Engineering Faculty, University of Mataram, Mataram, Indonesia, Indonesia*
[d] *Automotive Engineering Technology, Universitas Muhammadiyah Yogyakarta, Kasihan, Yogyakarta, Indonesia*
[e] *Informatics Study Program, Engineering Faculty, Telkom University, West Java,40257, Indonesia*
*Corresponding author: *agung.mulyo@esaunggul.ac.id*

***Abstract*— Along with the explosive growth of wireless communication network users who require large frequency bands and low latency, it is a challenge to create a new wireless communication network beyond 5G. This is because installing a massive 5G network requires a large investment by network providers. For this reason, the authors propose an alternative beyond 5G that has better quality than 5G and a relatively lower investment value than 5G networks. This study aims to analyze the downlink of the cooperative non-orthogonal multiple access (NOMA) network, which is usually used in 5G, combined with the use of a reconfigurable intelligence surface (RIS) antenna with decode and forward relay mechanisms. RIS is processed with a limited number of objects utilizing Rayleigh fading channels. The scenario is created by a user who relays without a direct link for users near the base station and with a direct link for users far from the base station. Under the Nakagami-*m* fading channel, the authors carefully evaluated the probability of loss for various users as a function of perfect channel statistical information (p-CSI) utilizing simply a single input-output (SISO) system with a finite number of RIS elements. As a key success metric, the efficiency of the proposed RIS-assisted NOMA transmission mechanism is evaluated through numerical data on the outage probability for each user. The modeling outcomes demonstrate that the RIS-aided NOMA network outperforms the traditional NOMA network.**

***Keywords*— Non-orthogonal multiple access (NOMA); outage probability (OP); p-CSI.**

Manuscript received 10 Apr. 2022; revised 27 Sep. 2022; accepted 20 Dec. 2022. Date of publication 10 Sep. 2023.

I. INTRODUCTION

Reconfigurable intelligent surfaces (RIS) are viewed as cutting-edge technology for the beyond fifth generation (B5G) communication system due to their potential to produce considerable increases in communication coverage, throughput, and energy effectiveness [1]-[6]. According to Liaskos et al. [7], due to the vast number of inexpensive reflecting devices that make up RIS, it is possible to cleverly rearrange the reflected signal propagation to meet specific communication objectives by changing the phase shifts of every reflecting unit [8], [9]. RIS is a planar meta-surface combined with a number of passive parts that can dynamically vary their reflections for various applications, including enhancing signal strength and reducing interference [10], [11]. In comparison to traditional techniques like active relaying and beam shaping. RIS reflects signals in a full-duplex and noise-free manner and significantly reduces energy consumption and hardware or deployment costs by utilizing only lightweight passive elements. [12], [13]. By altering the phase shifts of its passive components, RIS can artificially boost combined channel strengths and enlarge channel strengths using reflected electromagnetic waves [14].

Future wireless communication systems may benefit from NOMA, also known as non-orthogonal multiple access, which can assist several users inside a single resource part [15]-[17]. In conventional wireless networks without RIS, NOMA has concerned much attention and has shown to be an improvement over orthogonal multiple access (OMA) [18], [19]. NOMA can boost spectrum effectiveness while complementary user fairness and boosting network connections. The user of the robust channel employs a successive interference cancellation (SIC) approach prior to understanding the message in the downlink NOMA. This method aims to cancel out co-channel impedance from users on feebler channels [20].

Additionally, NOMA still needs to lower the energy required for the "amplify and forward" (AF) process to serve as a 5G basis. To remedy NOMA's inadequacies, a technology other than 5G is therefore required. The authors were motivated by this to create NOMA, which serves as the foundation for the 5G system that implements RIS-aided NOMA and realizes the ideas of the 6G system. [21], [22]. The feasible sum rate and outage probability for a downlink NOMA framework are covered in the reference [13]. The capacity to serve several customers at the same time, frequency, and code with varying degrees of power is the main benefit of NOMA over traditional OMA [23]-[25].

Many different channel types make up a Nakagami-*m* fading channel, with the Gaussian and Rayleigh fading channels serving as special cases. [26], [27]. Men, Ge, and Zhang [28] examined the performance of an AF relaying network based on NOMA. In terms of outage probability and ergodic sum rate, he discovered that NOMA outperformed OMA, while also providing greater spectral efficiency and user fairness than Nakagami-*m* fading channels. Cooperative NOMA delivers the same variety of direct and superior coding gains as cooperative OMA. It is also shown that assuming the relay has lower transmitted power than the base station, outage performance improved as the distance between the relay and the indirect link user decreased [11], [29], [30]. Gradshteyn and Ryzhik [31] were used to analyze the downlink NOMA system's outage performance with fixed power allocation. NOMA can offer customers with higher channel gains across Nakagami-*m* fading channels higher single rates than OMA [32], [33]. The majority of cooperative NOMA investigations up to this point have been conducted over Rayleigh fading channels in the p-CSI state. However, the channel estimate errors make them challenging to apply in practical wireless systems. Consequently, the authors proposed a study that is anticipated to contribute the following:

- The downlink system in NOMA supported by RIS can offer a reduced probability of blackout than conventional NOMA, according to the study's model scenario.
- Closed-form outage probability estimates for the RIS-assisted NOMA system are created. Since they are defined in terms of a wide range of various system parameters, it is possible to mathematically analyze how each system parameter affects the probability of an outage. For occurrence, the effect of the number of meta-surfaces in a RIS on the likelihood of an outage can be analyzed to improve the system's performance in actual operation. This study demonstrates that the number of meta-surfaces in RIS significantly impacts the system's outage probability.

II. Materials and Method

As seen in Fig. 1, we propose a two-user NOMA downlink based on RIS. A set of user groups is divided using orthogonal access. We suppose that each group contains representative users, such as a near-user (U_1) and a far-user (U_2), who are categorized according to their geographic location. The BS generates two beamforming vectors using the zero-force beamforming technique to serve two NOMA users. RIS-NOMA is helpful for developing various services since it can accommodate a wide range of Quality of Service (*QoS*) needs by grouping paired users. Once the user relies on the direct link connected to the BS, it becomes difficult.

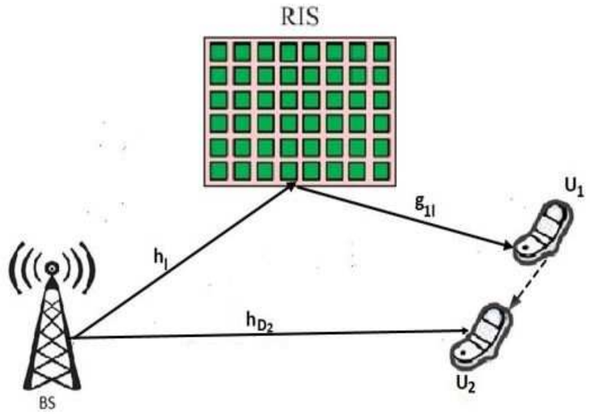

Fig. 1 The system models

Users U_1 and U_2 receive signals that are described by equations (1) and (2), respectively.

$$y_{U_1} = [\sum_{l=1}^{N} h_{1l} g_{1l} e^{j\Theta_l}](\sqrt{a_1 P_s} x_1 + \sqrt{a_2 P_s} x_2) + \omega_{U_1} + n_{U_1} \quad (1)$$

$$y_{U_2} = |h_{D_2}| \sqrt{P_s} x_2 + \omega_{U_2} + n_{U_2} \quad (2)$$

Where, ω_{U_1} is interference term from U_1 with $CN(0, \vartheta_1^2)$ and ϑ_1^2 is the constant. Additionally, n_{U1} and n_{U2} are AWGN noise terms, which are interference signals from outside sources that can be considered AWGN noise when combined with $CN(0, \Omega)$. The complex Gaussian channel vector terms for links *RIS*-U_1 and *BS*-*RIS*, respectively, are denoted by the symbols g_{1l} and h_l. User U_2 and the *BS* follow Rayleigh fading, while h_{D2} is the corresponding fading channel between them. The matrix θ_l ($l = N$) contains diagonal elements $exp(-j\theta_l)$ with θ_l standing for the reflection phase shift.

First, by performing SIC, the SINR of U_1 to detect x_2 is given as mentioned in Eq. (3), where, $\rho_s = \frac{P_s}{\omega}$. Then, the SINR at U_1 to detect x_1 is given as Eq. (4). U2 receives direct signal x2 from Base Station (BS). The SINR of U_2 to detect x_2 is given as Eq. (5).

$$SINR(U_{1,x_2 \to x_1}) = \gamma_{(U_{1,x_2 \to x_1})} = \frac{(|\sum_{l=1}^{N} |h_l||g_{1l}||^2) a_2 \rho_s}{(|\sum_{l=1}^{N} |h_l||g_{1l}||^2) a_1 \rho_s + \left(\frac{\eta_{SR}}{N}\left(d_{SR_1}^{-\chi}\right) . \frac{\eta_{RU_1}}{N}\left(d_{RU_1}^{-\chi}\right)\right) \rho_s + 1} \quad (3)$$

$$SINR(U_1, x_1) = \gamma_{(U_1, x_1)} = \frac{(|\sum_{l=1}^{N} |h_l||g_{1l}||^2) a_1 \rho_s}{(|\sum_{l=1}^{N} |h_l||g_{1l}||^2) a_1 \rho_s + \frac{\eta_{SR}}{N}\left(d_{SR}^{-\chi}\right) . \frac{\eta_{RU_1}}{N}\left(d_{RU_1}^{-\chi}\right) \rho_s + 1} \quad (4)$$

$$SINR(U_{2,BS}) = \gamma_{U_{2,BS}} = \frac{|h_{D_2}|^2 a_2 \rho_s}{a_1 \rho_s + \eta_{SU_2} d_{SU_2}^{-\chi} \rho_s + 1} \quad (5)$$

As shown in Fig. 1, a link is defined as the BS transmitting a signal to U1 via RIS. Two channels are available on this link, one from BS to RIS and the other from *RIS* to U_1. The U_2 is one user who receives a signal from BS via one of the channels. The notation denotes the fading channel from RIS to U1g_{1l}, while the channel's fading coefficient of *BS* to *RIS* is represented byh_l. Additionally, other links involve the BS communicating with U_2 via h_{D2}.

By using *RIS*, physically, the fading channel h_l and g_{1l} are related by $h_l^H \Phi g_{1l}$ relation, where Φ is denoted as phase shift. Using *RIS*, the fading channels h_l and g_{1l} are physically connected by the $h_l^H \Phi g_{1l}$ relation, where Φ stands for phase shift. The authors assume that the link is composed of several channels. Special instances of the Nakagami-*m* distribution's broad spectrum include the Gaussian channel and the Rayleigh channel. Therefore, it is assumed that each channel has a Nakagami-*m* distribution.

The general form of PDF for Nakagami-*m* distribution [34] for one channel function is mentioned by Eq.(6).

$$f_{|h|^2}(x) = \frac{m^m d^{\chi m} x^{m-1}}{(1-\eta)^m \Gamma(m)} e^{-\frac{m d^{\chi} x}{1-\eta}} \tag{6}$$

where, χ, η and m are path-loss coefficients, relative channel estimation error of channel and fading parameter, respectively. Because $\Gamma(m) = (m-1)!$, then Eq. (6) could be rewritten as Eq. (7)

$$f_{|\hat{h}|^2}(x) = \frac{m^m d^{\chi m} x^{m-1}}{(1-\eta)^m (m-1)!} e^{-\frac{m d^{\chi} x}{1-\eta}} \tag{7}$$

Cumulative Distribution Function (CDF) could be obtained by integrating the PDF above and expressed by Eq. (8)

$$F_{|h|^2}(x) = 1 - e^{-\frac{m d^{x} x}{1-\eta}} \sum_{i-0}^{m-1} \frac{1}{i!} \left(\frac{m d^{x} x}{1-\eta}\right)^i \tag{8}$$

Based on Eq. (7) and Eq. (8), we create the formula for calculating the connection outage probability for each user. Initially, let's assume that $\zeta_1$and $\zeta_2$stand in for the proper U_1 and U_2 target levels. The two SNR thresholds, $\rho_{Th_1}$and ρ_{Th_2} can be expressed as Equations. (9) and (10), respectively.

$$\rho_{Th_1} = \frac{(2^{2\zeta_1}-1)}{\rho_s} \tag{9}$$

$$\rho_{Th_2} = \frac{(2^{2\zeta_2}-1)}{\rho_s} \tag{10}$$

Equations (3) and (4) can be used to obtain it as τ_1 and τ_2, the first and second comparison parameters against the SNR threshold, resulting in the equations:
(*Proof*: see Appendix A.)

$$\tau_1 = \frac{\rho_{Th_1} \lambda_1}{(a_1 - a_1 \rho_{Th_1}) \rho_s} \tag{11}$$

$$\tau_2 = \frac{\rho_{Th_2} \lambda_1}{(a_2 - a_1 \rho_{Th_2}) \rho_s} \tag{12}$$

To achieve closed-form outage performance, a parameterX_v is defined as a gain in the channel coefficient of link v brought about by the implementation of RIS. If the RIS parts show random shifts, the definition $X_v = |h_l^H \phi g_{vl}|$ is applicable. Furthermore, we determine $\mathbb{E}\{X_v^2\} = \mathbb{E}\{|\widehat{X_v} + \omega_{U_2}|^2\}$and variance $\mathrm{Var}(X_v)$ are calculated in appendix A. Eq. (13) is used to express mv as the gamma distribution shape factor for the link v large-scale fading channel.

$$m_v = \frac{\mathbb{E}\{|X_v|^2\}}{Var(X_v)} \tag{13}$$

where m_1 and m_2 are the gamma distribution shape factors for the large-scale fading channel on U_1 and U_2, respectively, and v is the link index in this instance$v \in \{1,2\}$.
The following might be written for PDF and CDF by integrating RIS in the NOMA network.

$$f_{|\hat{X}_v|^2}(\tau) = (\delta_v)^{m_v} \frac{\tau^{m_v-1}}{(m_v-1)!} e^{-\delta_v \tau} \tag{14}$$

$$F_{|\hat{X}_v|^2}(\tau) = 1 - e^{-\delta_v \tau} \sum_{i-0}^{m_v-1} \frac{1}{i!} (\delta_v \tau)^i \tag{15}$$

The additional events of the outage in this study take place at U_1. When U_1 correctly decodes both the signal x_2 and its own signal x_1, Eq. (16) could be used to express the outage probability of U_1.

$$P_{U_1} = 1 - Pr(\gamma_{(U_1,x_2)} > \rho_{Th_2}, \gamma_{(U_1,x_1)} > \rho_{Th_1}) \tag{16}$$

It is defined $\omega_{U_1}$is path-loss distance-induced attenuation. Because each channel suffers attenuation and noise, the link BS → U1 through RIS, which decodes itself signal x_1 could be determined as a parameter λ_1 is mentioned as Eq. (17).

$$\lambda_1 = \frac{\eta_{SR}}{N} (d_{SR}^{-\chi}) . \frac{\eta_{RU_1}}{N} (d_{RU_1}^{-\chi}) \rho_s + 1 \tag{17}$$

where λ_v denotes the noise and attenuation brought on by each user's use of RIS-aided equipment. By defining $a_1 + a_2 = 1$ where $a_2 > a_1$ then Eq. (16) could be expressed as Eq. (18).

$$P_{U_1} = 1 - e^{-\delta_1 \tau} \sum_{j-0}^{m_1-1} \frac{(\delta_1 \tau)^j}{j!} \tag{18}$$

where, m_1, τ_1,τ_2,λ_1 and δ_1 are shown in Eq. (19), Eq. (11), Eq. (12), Eq. (17), and Eq. (20), respectively.

$$m_1 = \frac{(2N^2+2N)\beta_{RU_1}^2 \beta_{SR}^2 + \left|\frac{\eta_{SR}}{N}(d_{SR}^{-\chi}) . \frac{\eta_{RU_v}}{N}(d_{RU_1}^{-\chi})\right|^2}{(N^2+2N)\beta_{RU_1}^2 \beta_{SR}^2 - 2N\beta_{SR}\beta_{RU_1} \frac{\eta_{SR}}{N}(d_{SR}^{-\chi}) . \frac{\eta_{RU_v}}{N}(d_{RU_1}^{-\chi})} \tag{19}$$

$$\delta_1 = \frac{m_1}{N} \left(\frac{d_{SR}^{\chi}}{1-\eta_{SR}} + \frac{d_{RU_1}^{\chi}}{1-\eta_{RU_1}}\right) \tag{20}$$

The outage probability at U_1 could then be expressed in Eq. (21).

$$P_{U_1} = 1 - e^{-\frac{m_1}{N}\left(\frac{d_{SR}^{\chi}}{1-\eta_{SR}} + \frac{d_{RU_1}^{\chi}}{1-\eta_{RU_1}}\right)\tau} \sum_{j-0}^{m_1-1} \frac{\left(\frac{m_1}{N}\left(\frac{d_{SR}^{\chi}}{1-\eta_{SR}} + \frac{d_{RU_1}^{\chi}}{1-\eta_{RU_1}}\right)\tau\right)^j}{j!} \tag{21}$$

(*Proof*: See in Appendix A.)

Similar reasoning might be used to determine the likelihood of an outage at U_2. According to the system model, the received signals which are received by U_2 consist of direct signals from *BS* and rely on a signal from U_1. The relying signal from U_1 is the link *BS* → U_1 through *RIS,* which decodes signal x_2 for U_2, which has and could be mentioned as Eq. (16) above. We give the symbols dash-line the system model for this link, and there is no received signal by x_2 from *RIS*. Furthermore, the direct signal from *BS* to U_2 that has SNR as Eq. (5).

The first of two occurrences that make up the outage probability at U_2 is the inability of U_1 to decode the signal x_2. In addition, in the second instance, U_2 is unable to decode its own signal x_2 from BS, while U_1 can positively decode the signal x_2. In light of these occurrences, the following equation can be used to express the U_2 outage probability.

$$P_{U_2} = 1 - e^{-(\delta_1\tau_2+\delta_3\tau_4)} \sum_{j=0}^{m_1-1} \sum_{k=0}^{m_3-1} \frac{(\delta_1\tau_2)^j(\delta_3\tau_4)^k}{j!k!} \quad (22)$$

$$m_2 = \frac{2\beta_{SU_2}^2+4N\beta_{SU_2}\beta_{SR}\beta_{RU_2}+(2N^2+2N)\beta_{RU_2}^2\beta_{SR}^2+|\Psi_2|^2}{\beta_{SU_2}^2+2N\beta_{SU_2}\beta_{SR}\beta_{RU_2}+(N^2+2N)\beta_{RU_2}^2\beta_{SR}^2-2(\beta_{SU_2}+N\beta_{SR}\beta_{RU_2})\Psi_2} \quad (23)$$

where, $\Psi_2 = \eta_{SU_2}.\left(d_{SU_2}^{-\chi}\right) + \frac{\eta_{SR}}{N}\left(d_{SR}^{-\chi}\right).\frac{\eta_{RU_v}}{N}\left(d_{RU_2}^{-\chi}\right)$.

By inputting τ_2 in Eq. (12), λ_1 in Eq. (17), m_2 in Eq. (23), τ_4 in Eq. (24), λ_3 in Eq. (25), δ_3 in Eq. (26), and $m_3 = 2$ then the outage probability in Eq. (22) could be solved.

$$\tau_4 = \frac{\lambda_3\rho_{Th_2}}{(a_2-a_1\rho_{Th_2})\rho_s} \quad (24)$$

$$\lambda_3 = \eta_{SU_2}\left(d_{SU_2}^{-\chi}\right) + 1 \quad (25)$$

Next, the δ_3 is stated as Eq. (26).

$$\delta_3 = \frac{m_2}{N}\left(\frac{d_{SR}^{\chi}}{1-\eta_{SR}} + \frac{d_{RU_2}^{\chi}}{1-\eta_{RU_2}}\right) \quad (26)$$

τ_4 is fourth-comparison-parameter against to SNR threshold. The link's gamma distribution at U_1, U_2 has scale factors δ_1, δ_3.
(*Proof*: see in Appendix-B).

III. Result and Discussion

In this part, the outage probability is simulated using mathematical derivations, and the simulation is validated using a Monte-Carlo simulation. Table 1 specifies the simulation parameters that will be used in the numerical simulation. Furthermore, the large-scale fading coefficient [dB] at near-user and far-user locations is modeled by β_k.

$$\beta_k = G_t + G_r + 10\chi_k \log_{10}\left(\frac{d_k}{1m}\right) - 30 + z_k \quad (27)$$

where, $k \in \{SU_1, SR, RU_1, SU_2, SR, RU_2, U_1U_2\}$ and z_k is the shadow fading. Additionally, simulations are produced by changing settings in the MATLAB programming language. Monte Carlo simulations are used to validate the exact expressions of the outage probability. The previous investigations' findings were numerically supported by mapping the sites into the Cartesian coordinate system.

TABLE I
SIMULATION PARAMETERS

Description	Parameter
Power allocation coefficient	$a_1 = 0.2$, $a_2 = 0.8$
Path-loss exponent	$\chi_k = 2$
Relative-channel estimation error	$\eta_k = 1 \times 10^{-4} \sim 9 \times 10^{-4}$;
Distance between two nodes	$d_{SU_1} = 0.04(50m), d_{SR_1} = d_{SR_2} = 0.06(60m)$, $d_{RU_1} = 0.02, d_{SU_2} = 0.04, d_{RU_2} = 0.04$, $d_{U_1U_2} = 1 - d_{SU_1}$
Transmit SNR	$\rho_s = 0 \sim 60dB$
The antenna gains at transmitter and receiver	$G_t = 3.2dB_i, G_r = 1.3dB_i$
Target Rate	$\zeta_1 = 3.6BPCU, \zeta_2 = 1BPCU$

For user U_1, Fig. 2 displays the simulation and analytical findings of the outage performance against SNR while using the RIS on the NOMA network for various RIS element counts. The outage performance versus SNR by NOMA Network is also compared. The graph clearly shows that as the number of RIS pieces rises, the probability of an outage falls. The NOMA network's RIS implementation performs better during outages after the installation of RIS components. Additionally, it performs better than the NOMA outage performance of the network system. This demonstrates that the suggested RIS-NOMA system performs effectively, as predicted by our study.

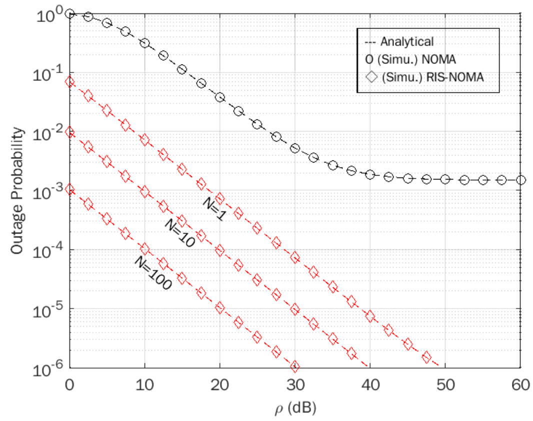

Fig. 2 The Outage probability for U_1

For user U_2, Fig. 3 displays the outage probability versus SNR simulation results and analytical findings without RIS. Additionally, the SNR of U_2 is used to compare NOMA Network's outage performance to that of U_2. We can see that the proposed system performs well without RIS-NOMA since U_2 just receives the signal through the relaying link and receives the signals as direct links, enhancing signal dependability. According to our research, U_2 performs better during outages when there are more RIS elements.

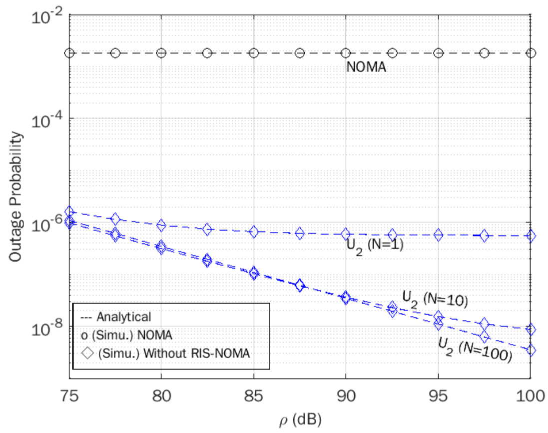

Fig. 3 The Outage-probability for U_2

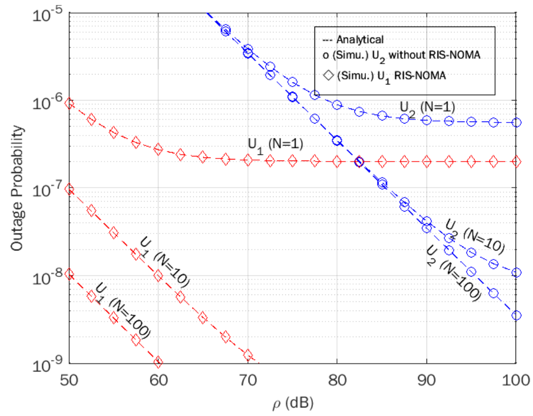

Fig. 4 Comparison of the Outage probability between U_1 and U_2

Furthermore, it is evident from the aforementioned two figures that U_2's outage probability outperforms that of U_1. Fig. 4 compares the outage probability versus SNR for various numbers of RIS elements for near-user U_1 and far-user U_2 based on simulation and analytical results. In this comparison, it is clear that the near-user U_1 performs significantly better than the far-user U_2 as the number of RIS elements grows. It proves that even without *amplification and forward* (AF) mode, the RIS implementation on the NOMA network can outperform the NOMA network in terms of outage performance. The only mode utilized is decoded and forward (DF).

IV. Conclusion

In this study, we deduced how well a RISNOMA system performed during an outage. The closed-form equation was discovered for the probability of an outage for users U1 without a direct link and U2 with a direct link. We simplified the system performance study on the gap between two users by assuming *Nakagami - m* with p-CSI, and this paper only focuses on the major performance parameter, outage probability. To confirm the correctness of our formulas, Monte Carlo simulations are performed. Future development will take multiple users at the RIS-NOMA system into consideration.

References

[1] Z. Yang, Z. Ding, P. Fan, and G. K. Karagiannidis, "On the performance of non-orthogonal multiple access systems with partial channel information," *IEEE Transactions on Communications,* vol. 64, no. 2, pp. 654-667, 2015.

[2] Z. Ding, X. Lei, G. K. Karagiannidis, R. Schober, J. Yuan, and V. K. Bhargava, "A survey on non-orthogonal multiple access for 5G networks: Research challenges and future trends," *IEEE Journal on Selected Areas in Communications,* vol. 35, no. 10, pp. 2181-2195, 2017.

[3] Y. Zhang, H. Zhao, L. Yuan, and H. Chen, "Slip ratio estimation for electric vehicle with in-wheel motors based on EKF without detection of vehicle velocity," in *2016 Chinese Control and Decision Conference (CCDC)*, 2016: IEEE, pp. 4427-4432.

[4] Q. Wu and R. Zhang, "Intelligent reflecting surface enhanced wireless network via joint active and passive beamforming," *IEEE Transactions on Wireless Communications,* vol. 18, no. 11, pp. 5394-5409, 2019.

[5] M. Di Renzo *et al.*, "Smart radio environments empowered by reconfigurable AI meta-surfaces: An idea whose time has come," *EURASIP Journal on Wireless Communications and Networking,* vol. 2019, no. 1, pp. 1-20, 2019.

[6] Q. Wu and R. Zhang, "Beamforming optimization for intelligent reflecting surface with discrete phase shifts," in *ICASSP 2019-2019 IEEE International Conference on Acoustics, Speech and Signal Processing (ICASSP)*, 2019: IEEE, pp. 7830-7833.

[7] C. Liaskos, S. Nie, A. Tsioliaridou, A. Pitsillides, S. Ioannidis, and I. Akyildiz, "A new wireless communication paradigm through software-controlled metasurfaces," *IEEE Communications Magazine,* vol. 56, no. 9, pp. 162-169, 2018.

[8] L. Dai, B. Wang, Y. Yuan, S. Han, I. Chih-Lin, and Z. Wang, "Non-orthogonal multiple access for 5G: solutions, challenges, opportunities, and future research trends," *IEEE Communications Magazine,* vol. 53, no. 9, pp. 74-81, 2015.

[9] P. Xu, G. Chen, G. Pan, and M. Di Renzo, "Ergodic secrecy rate of RIS-assisted communication systems in the presence of discrete phase shifts and multiple eavesdroppers," *IEEE Wireless Communications Letters,* vol. 10, no. 3, pp. 629-633, 2020.

[10] H.-C. Chen, K. T. Putra, S.-S. Tseng, C.-L. Chen, and J. C.-W. Lin, "A spatiotemporal data compression approach with low transmission cost and high data fidelity for an air quality monitoring system," *Future Generation Computer Systems,* vol. 108, pp. 488-500, 2020.

[11] C.-B. Le, D.-T. Do, X. Li, Y.-F. Huang, H.-C. Chen, and M. Voznak, "Enabling NOMA in backscatter reconfigurable intelligent surfaces-aided systems," *IEEE Access,* vol. 9, pp. 33782-33795, 2021.

[12] Z. Zhang, K. Long, A. V. Vasilakos, and L. Hanzo, "Full-duplex wireless communications: Challenges, solutions, and future research directions," *Proceedings of the IEEE,* vol. 104, no. 7, pp. 1369-1409, 2016.

[13] Z. Ding, M. Peng, and H. V. Poor, "Cooperative non-orthogonal multiple access in 5G systems," *IEEE Communications Letters,* vol. 19, no. 8, pp. 1462-1465, 2015.

[14] X. Yue, Y. Liu, S. Kang, A. Nallanathan, and Z. Ding, "Exploiting full/half-duplex user relaying in NOMA systems," *IEEE Transactions on Communications,* vol. 66, no. 2, pp. 560-575, 2017.

[15] Y. Liu, Z. Ding, M. Elkashlan, and H. V. Poor, "Cooperative non-orthogonal multiple access with simultaneous wireless information and power transfer," *IEEE Journal on Selected Areas in Communications,* vol. 34, no. 4, pp. 938-953, 2016.

[16] X. Liu, X. Wang, and Y. Liu, "Power allocation and performance analysis of the collaborative NOMA assisted relaying systems in 5G," *China Communications,* vol. 14, no. 1, pp. 50-60, 2017.

[17] L. Song, Y. Li, Z. Ding, and H. V. Poor, "Resource management in non-orthogonal multiple access networks for 5G and beyond," *IEEE Network,* vol. 31, no. 4, pp. 8-14, 2017.

[18] B. Zheng, Q. Wu, and R. Zhang, "Intelligent reflecting surface-assisted multiple access with user pairing: NOMA or OMA?," *IEEE Communications Letters,* vol. 24, no. 4, pp. 753-757, 2020.

[19] Y. Cheng, K. H. Li, Y. Liu, K. C. Teh, and H. V. Poor, "Downlink and uplink intelligent reflecting surface aided networks: NOMA and OMA," *IEEE Transactions on Wireless Communications,* vol. 20, no. 6, pp. 3988-4000, 2021.

[20] Y. Zhang, J. Ge, and E. Serpedin, "Performance analysis of non-orthogonal multiple access for downlink networks with antenna selection over Nakagami-m fading channels," *IEEE Transactions on Vehicular Technology,* vol. 66, no. 11, pp. 10590-10594, 2017.

[21] N. T. Do, D. B. Da Costa, T. Q. Duong, and B. An, "A BNBF user selection scheme for NOMA-based cooperative relaying systems with SWIPT," *IEEE Communications Letters,* vol. 21, no. 3, pp. 664-667, 2016.

[22] A. Hemanth, K. Umamaheswari, A. C. Pogaku, D.-T. Do, and B. M. Lee, "Outage performance analysis of reconfigurable intelligent surfaces-aided NOMA under presence of hardware impairment," *IEEE Access,* vol. 8, pp. 212156-212165, 2020.

[23] Z. Ding, Z. Yang, P. Fan, and H. V. Poor, "On the performance of non-orthogonal multiple access in 5G systems with randomly deployed users," *IEEE signal processing letters,* vol. 21, no. 12, pp. 1501-1505, 2014.

[24] Y. Saito, A. Benjebbour, Y. Kishiyama, and T. Nakamura, "System-level performance of downlink non-orthogonal multiple access (NOMA) under various environments," in *2015 IEEE 81st vehicular technology conference (VTC Spring)*, 2015: IEEE, pp. 1-5.

[25] Y. Saito, A. Benjebbour, Y. Kishiyama, and T. Nakamura, "System-level performance evaluation of downlink non-orthogonal multiple access (NOMA)," in *2013 IEEE 24th Annual International Symposium on Personal, Indoor, and Mobile Radio Communications (PIMRC)*, 2013: IEEE, pp. 611-615.

[26] T. Hou, X. Sun, and Z. Song, "Outage performance for non-orthogonal multiple access with fixed power allocation over Nakagami-${m}$ fading channels," *IEEE Communications Letters,* vol. 22, no. 4, pp. 744-747, 2018.

[27] L. Lv, Q. Ni, Z. Ding, and J. Chen, "Application of non-orthogonal multiple access in cooperative spectrum-sharing networks over Nakagami-$ m $ fading channels," *IEEE Transactions on Vehicular Technology,* vol. 66, no. 6, pp. 5506-5511, 2016.

[28] J. Men, J. Ge, and C. Zhang, "Performance analysis of non-orthogonal multiple access for relaying networks over Nakagami-$ m $ fading channels," *IEEE Transactions on Vehicular Technology,* vol. 66, no. 2, pp. 1200-1208, 2016.

[29] X. Liang, Y. Wu, D. W. K. Ng, Y. Zuo, S. Jin, and H. Zhu, "Outage performance for cooperative NOMA transmission with an AF relay," *IEEE Communications Letters,* vol. 21, no. 11, pp. 2428-2431, 2017.

[30] T. L. Nguyen and D. T. Do, "Power allocation schemes for wireless powered NOMA systems with imperfect CSI: An application in multiple antenna–based relay," *International Journal of Communication Systems,* vol. 31, no. 15, p. e3789, 2018.

[31] I. S. Gradshteyn and I. M. Ryzhik, *Table of integrals, series, and products*. Academic press, 2014.

[32] L. Liu, C. Yuen, Y. L. Guan, and Y. Li, "Capacity-achieving iterative LMMSE detection for MIMO-NOMA systems," in *2016 IEEE International Conference on Communications (ICC)*, 2016: IEEE, pp. 1-6.

[33] H. Poor, "Application of Non-Orthogonal Multiple Access in LTE and 5G Networks," *IEEE Communications Magazine Articles News & Events of Interest to Communications Engineers,* 2017.

[34] X. Gong, X. Yue, and F. Liu, "Performance analysis of cooperative NOMA networks with imperfect CSI over Nakagami-m fading channels," *Sensors,* vol. 20, no. 2, p. 424, 2020.

[35] H.-C. Chen, A. M. Widodo, J. C.-W. Lin, and C.-E. Weng, "Reconfigurable Intelligent Surface-Aided Cooperative NOMA with p-CSI Fading Channel toward 6G-Based IoT System," *Sensors,* vol. 22, no. 19, p. 7664, 2022.

APPENDIX A
PROOF OF PROPOSITION

It is described, $X_v = |\sum_{l=1}^{N} h_{vl}^H \Phi g_{vl}|^2$. In the event that it is thought that the signal reflected by the RIS components contains random phase fluctuations. It is acceptable to suppose that $\hat{h}_l \sim \mathbb{CN}(0, \beta_{SR} I_N)$, $\hat{g}_{vl} \sim \mathbb{CN}(0, \beta_{RU_v} I_N)$and $\phi = diag(e^{j\theta_1}, e^{j\theta_2}, \ldots, e^{j\theta_N})$, where I_N and $\theta_n \in [-\pi, \pi]$are character matrices of order N with a range for θ_n, respectively, due to the identical independent distribution of each channel (i.i.d). In addition, we define the anticipated value. The independence of the channels that make up $\mathbb{E}\{|X_v|\}$ are averaged. Eq could be used to express it (A.1).

$$\mathbb{E}\{|X_v|\} = \mathbb{E}\left\{\left|h_l^H \Phi g_{vl}\right|^2\right\} \quad (A.1)$$

$X_v$can be written as an equation and represents the average link $\hat{X}_v$ and fade due to path-loss distance-induced attenuation $\sigma_{e_v}^2$ in the propagation location (A.2).

$$\mathbb{E}\{|X_v|\} = \mathbb{E}\{\hat{X}_v + \sigma_{e_v}^2\} = \mathbb{E}\{\hat{X}_v\} + \sigma_{e_v}^2 \quad (A.2)$$

Path-loss distance-induced attenuation $\sigma_{e_v}^2$ could be defined as $\frac{\eta_{SR}}{N}(d_{SR}^{-\chi}).\frac{\eta_{RU_v}}{N}(d_{RU_v}^{-\chi})$, then Eq. (A.2) might be revised as Eq. (A.3).

$$\mathbb{E}\{|X_v|\} = \mathbb{E}\left\{\left|\hat{h}_l^H \Phi \hat{g}_{vl}\right|^2\right\} + \frac{\eta_{SR}}{N}(d_{SR}^{-\chi}).\frac{\eta_{RU_v}}{N}(d_{RU_v}^{-\chi}) \quad (A.3)$$

We define that $\mathbb{E}\left\{\left|\hat{h}_l^H \Phi \hat{g}_{vl}\right|^2\right\} = N\beta_{SR}\beta_{RU_v}$, so that Eq. (A.3) could be written as Eq. (A.4)

$$\mathbb{E}\{|X_v|\} = N\beta_{SR}\beta_{RU_v} + \frac{\eta_{SR}}{N}(d_{SR}^{-\chi}).\frac{\eta_{RU_v}}{N}(d_{RU_v}^{-\chi}) \quad (A.4)$$

Furthermore, it is determined $\mathbb{E}\left\{\left|\hat{X}_v\right|^2\right\}$as Eq. (A.5) below.

$$\mathbb{E}\left\{\left|\hat{X}_v\right|^2\right\} = \mathbb{E}\left\{\left|\hat{h}_l^H \Phi \hat{g}_{vl}\right|^2\right\} \quad (A.5)$$

Using the circular symmetric properties, Eq. (A.5) could be written as Eq. (A.6).

$$\mathbb{E}\left\{\left|\hat{X}_v\right|^2\right\} = \mathbb{E}\left\{||\Phi \hat{g}_{vl}||^4 \left|\frac{\hat{h}_l^H \Phi \hat{g}_{vl}}{||\Phi \hat{g}_{vl}||}\frac{\hat{g}_{vl}^H \Phi^H \hat{h}_l}{||\Phi \hat{g}_{vl}||}\right|^2\right\} \quad (A.6)$$

If it is defined $z = \frac{\hat{h}_l^H \Phi \hat{g}_{vl}}{||\Phi \hat{g}_{vl}||}$; $z \sim CN(0, \beta_{SR})$, then

$$\mathbb{E}\left\{\left|\hat{X}_v\right|^2\right\} = \mathbb{E}\left\{||\Phi \hat{g}_{vl}||^4 |z|^4\right\} = \mathbb{E}\left\{||\Phi \hat{g}_{vl}||^4\right\}\mathbb{E}\{|z|^4\} \quad (A.7)$$

We could get Eq. (A.24) by entering the values $\mathbb{E}\left\{||\Phi \hat{g}_{vl}||^4\right\}\mathbb{E}\{|z|^4\}$ into Eq (A.6).

It can also be described as $X_v = \hat{X}_v + e_v = \hat{X}_v + \sigma_{e_v}^2$, allowing the expected-value of ${X_v}^2$ to express in the form of Eq. (A.8).

$$\mathbb{E}\left\{\left|\hat{X}_v\right|^2\right\} = N(N+1)\beta_{RU_v}^2 2\beta_{SR}^2 = (2N^2 + 2N)\beta_{RU_v)}^2\beta_{SR}^2 \quad (A.8)$$

Based on Eq. (A.8), we specify $\mathbb{E}\{|X_v|^2\} = \mathbb{E}\left\{\left|\hat{X}_v\right|^2\right\} + \sigma_{e_v}^2$and could be rewritten as Eq. (A.9) ad Eq. (A.10).

$$\mathbb{E}\{|X_v|^2\} = \mathbb{E}\left\{\left|\left|\hat{h}_l^H \Phi \hat{g}_{vl}\right|^2 + \left|\frac{\eta_{SR}}{N}(d_{SR}^{-\chi}).\frac{\eta_{RU_v}}{N}(d_{RU_v}^{-\chi})\right|\right|^2\right\} \quad (A.9)$$

$$\mathbb{E}\{|X_v|^2\} = (2N^2 + 2N)\beta_{RU_v}^2\beta_{SR}^2 + \left|\frac{\eta_{SR}}{N}(d_{SR}^{-\chi}).\frac{\eta_{RU_v}}{N}(d_{RU_v}^{-\chi})\right|^2 \quad (A.10)$$

By defining, $Var\{|X_v|\} = E\{|X_v|^2\} - |E\{|X_v|\}|^2$, then it may be said to be as Eq.(A.11).

$$Var\{|X_v|\} = (N^2 + 2N)\beta_{RU_v}^2\beta_{SR}^2 - 2N\beta_{SR}\beta_{RU_v}\frac{\eta_{SR}}{N}(d_{SR}^{-\chi}).\frac{\eta_{RU_v}}{N}(d_{RU_v}^{-\chi}) \quad (A.11)$$

Next,$\tau_1$in Eq. (11) could be derived by defining ρ_{Th_1}as Eq. (A.12).

$$\rho_{Th_1} = \frac{(2^{2\zeta_1} - 1)}{\rho_s} \quad (A.12)$$

From Eq. (7), we define the notation $A_1 = \left|\sum_{l=1}^{L}|\hat{h}_l||\hat{g}_{1l}|\right|^2and\lambda_1 = \frac{\eta_{SR}}{N}(d_{SR}^{-\chi}).\frac{\eta_{RU_1}}{N}(d_{RU_1}^{-\chi})\rho_s + 1$ so that it can be rewritten Eq. (7) as Eq. (A.18).

$$\frac{A_1 a_1 \rho_s}{A_1 a_1 \rho_s + \lambda_1} \geq \rho_{Th_1} \quad (A.13)$$

$$\Rightarrow A_1 a_1 \rho_s \geq (A_1 a_1 \rho_s + \lambda_1)\rho_{Th_1} \quad (A.14)$$

$$\Rightarrow A_1 a_1 \rho_s - A_1 a_1 \rho_s \rho_{Th_1} \geq \lambda_1 \rho_{Th_1} \quad (A.15)$$

$$\Rightarrow A_1 \rho_s (a_1 - a_1 \rho_{Th_1}) \geq \lambda_1 \rho_{Th_1} \quad (A.16)$$

$$\Rightarrow A_1 \geq \frac{\lambda_1 \rho_{Th_1}}{(a_1 - a_1 \rho_{Th_1})\rho_s} \quad (A.17)$$

$$\Rightarrow \tau_1 = \frac{\lambda_1 \rho_{Th_1}}{(a_1 - a_1 \rho_{Th_1})\rho_s} \quad (A.18)$$

Similarly, it is defined ρ_{Th_2}in Eq. (A.19).

$$\rho_{Th_2} = \frac{(2^{2\zeta_2} - 1)}{\rho_s} \quad (A.19)$$

then, $\tau_2$could be derived from Eq. (A.19) as follows.

$$\frac{A_2 a_2 \rho_s}{A_2 a_1 \rho_s + \lambda_1} \geq \rho_{Th_2} \quad (A.20)$$

$$\Rightarrow A_2 a_2 \rho_s \geq (A_2 a_1 \rho_s + \lambda_1)\rho_{Th_2} \quad (A.21)$$

$$\Rightarrow A_2 a_2 \rho_s - A_2 a_1 \rho_s \rho_{Th_2} \geq \lambda_1 \rho_{Th_2} \quad (A.22)$$

$$\Rightarrow A_2 \rho_s (a_2 - a_1 \rho_{Th_2}) \geq \lambda_1 \rho_{Th_2} \quad (A.23)$$

$$\Rightarrow A_2 \geq \frac{\lambda_1 \rho_{Th_2}}{(a_2 - a_1 \rho_{Th_2})\rho_s} \quad (A.24)$$

$$\Rightarrow \tau_2 = \frac{\lambda_1 \rho_{Th_2}}{(a_2 - a_1 \rho_{Th_2})\rho_s} \quad (A.25)$$

The outage probability at user U_1 could be mentioned in Eq. (A.26), which is determined by making changes to the equations of PDF and CDF given above as a result of the deployment of RIS in NOMA networks.

$$P_{U_1} = 1 - Pr\left(\left|\hat{X}_1\right|^2 > \tau_2, \left|\hat{X}_1\right|^2 > \tau_1\right) \quad (A.26)$$

so that, by rearranging Eq. (A.26) obtained as Eq. (A.27).

$$P_{U_1} = 1 - Pr\left(\left|\hat{X}_1\right|^2 > max(\tau_2, \tau_1)\right) \quad (A.27)$$

$$P_{U_1} = 1 - \left(\left|\hat{X}_1\right|^2 > \tau\right) \quad (A.28)$$

where, according to which value is the highest, τ might be as high as $\tau_2$orτ_1. The reason for this is that there is a higher probability that U_1 will not successfully decode the signal x_2 from another user, U_2, or its signal, x_2, than that any of those two events will occur. Consequently, Eq. (A.27) is written as Eq. (A.28).

APPENDIX B
PROOF OF PROPOSITION

According to the equation of $\gamma_{U_{2,BS}}$, in the Eq. (B.1).

$$\gamma_{U_{2,BS}} = \frac{|h_{D_2}|^2 a_2\rho_s}{a_1\rho_s+\eta_{SU_2}\, d_{SU_2}^{-\chi}\rho_s+1} \qquad (B.1)$$

We derive τ_4 base on the system model, which could be conducted as follows.

If it is defined $B = |\hat{h}_{D_2}|^2$ and $\lambda_3 = \eta_{SU_2}(\,d_{SU_2}^{-\chi})\rho_s + 1$, then

$$\Rightarrow \frac{|\hat{h}_{D_2}|^2 a_2\rho_s}{|\hat{h}_{D_2}|^2 a_1\rho_s+\eta_{SU_2}(\,d_{SU_2}^{-\chi})\rho_s+1} \geq \rho_{Th_2} \qquad (B.2)$$

$$\Rightarrow \frac{Ba_2\rho_s}{Ba_1\rho_s+\lambda_3} \geq \rho_{Th_2} \qquad (B.3)$$

$$\Rightarrow Ba_2\rho_s \geq (Ba_1\rho_s + \lambda_3)\rho_{Th_2} \qquad (B.4)$$

$$\Rightarrow Ba_2\rho_s - Ba_1\rho_s\rho_{Th_2} \geq \lambda_3\rho_{Th_2} \qquad (B.5)$$

$$\Rightarrow B\rho_s(a_2 - a_1\rho_{Th_2}) \geq \lambda_3\rho_{Th_2} \qquad (B.6)$$

$$\Rightarrow B \geq \frac{\lambda_3\rho_{Th_2}}{(a_2-a_1\rho_{Th_2})\rho_s} \qquad (B.7)$$

$$\Rightarrow \tau_4 = \frac{\lambda_3\rho_{Th_2}}{(a_2-a_1\rho_{Th_2})\rho_s} \qquad (B.8)$$

The outage probability at user U_2 could be shown as follows.

$$P_{U_2} = Pr(\gamma_{U_{2,BS}} < \gamma_{Th_2}) + Pr(\gamma_{U_{2,BS}} > \gamma_{Th_2}, \gamma_{U_{2,U_1}} < \gamma_{Th_2}) \qquad (B.9)$$

$$P_{U_2} = Pr(\gamma_{U_{2,BS}} < \gamma_{Th_2}) + Pr(\gamma_{U_{2,BS}} > \gamma_{Th_2})\, Pr(\gamma_{U_{2,U_1}} < \gamma_{Th_2}) \qquad (B.10)$$

$$P_{U_2} = 1 - Pr(\gamma_{U_{2,BS}} > \gamma_{Th_2})\, Pr(\gamma_{U_{2,U_1}} > \gamma_{Th_2}) \qquad (B.11)$$

$$P_{U_2} = 1 - e^{-\delta_1\tau_2}\sum_{j-0}^{m_1-1}\frac{(\delta_1\tau_2)^j}{j!}\, e^{-\delta_3\tau_4}\sum_{k=0}^{m_3-1}\frac{(\delta_3\tau_4)^k}{k!} \qquad (B.12)$$

NOTATION

TABLE OF NOTATION [35].

Notation	Definition
$s(t)$	A superimposed signal is sent to both the near (U_1) and far (U_2) users.
P_s	Transmitted signal power
P_1	Transmitted signal power by U_1
a_1 and a_2	Power level x_1 and x_2
N	The quantity of RIS components
α	The RIS Reflected Signal's Amplitude Coefficient with $\alpha \in (0,1]$
θ_l	Phase modification is possible with the *l-th* reflected element of RIS.
Φ	The *phase-shift matrix*, diag(exp(jθ_1), exp(jθ_2), …, exp(jθ_L))
$(.)^H$	Hermitian transpose
β_k	The large-scale fading coefficients of the channel *k*
Ω_k	The link power of channel *k*
$\hat{\Omega}_k$	Average-connection power of channel *k*
$\hat{h}_k$	Average-fading coefficient of channel *k*
h_k	Fading-coefficient of channel *k*
$\hat{X}_v$	Average fading-coefficient gain by RIS of *v* user
X_v	Gain in fading coefficient by *v* user's RIS
e_k	Channel estimation error
$\sigma_{e_k}^2$	Channel estimation error variant
η_k	Channel k with relative channel estimation error
m_v	The gamma distribution channel's shape factor
χ	Path-loss exponent
d_k	Distance of two-points crossed by channel *k*
$P_{(..)}$	Outage probability at (..)
n_{U_1} and n_{U_2}	AWGN at U_1 and U_2.
$d_{SU_1}, d_{SR_1}, d_{RU_1}$	Distance of BS − U_1, BS − RIS, and RIS − U_1
$d_{SU_2}, d_{SR_2}, d_{RU_2}$	Distance of BS − U_2, BS − RIS, and RIS − U_2
$h_{D_1}, h_{D_2}, h_l, g_{1l}, g_{2l}$	Coefficients of fading channel
ρ_s	Transmit signal-to-noise ratio (SNR)
$\rho_{U_2 \to U_1}$	At U_1, examine the incoming signal for interference and noise ratio in order to decode it (SINR).
ρ_{U_1}, ρ_{U_2}	The received SINR of U_1 and U_2 to decode the signal itself.
$\rho_{2,U2}$	The received SINR of U_2 to decode the signal x_2 to relay link
$\rho_{U_2}^{SC}$	The received SINR after selection combining (SC) at U_2
ρ_{Th_1} and ρ_{Th_2}	SINR target of user U_1 and U_2
R_1 and R_2	Target rate of user U_1 and U_2
P_{U_1} and P_{U_2}	Outage probability of U_1 and U_2
τ_1, τ_2 and τ_3	The first-comparison parameter, the second-comparison parameter, and the third-comparison parameter are all variables.
λ_1, λ_2	Interference and noise due to the using of RIS-aided of U_1 and U_2
δ_1, δ_2	Scale factor of the gamma-distribution of the channel of U_1 and U_2